RESEARCH ARTICLE

Hybridization and absorption properties of surface plasmon polaritons in metal nanostructures

Ruirui Zhang*

School of Computer Science and Technology, Shandong University of Finance and Economics, Jinan, Shandong, China

Received: October 18, 2023; **accepted:** December 15, 2023.

Surface plasmon polaritons (SPPs) are oscillations of electrons at the interface between a metal and a dielectric material, induced by incident light. They are applied in nanophotonics and plasmonics, enhancing light-matter interactions for the development of devices like sensors and optoelectronics. The research results of SPPs of metal nanostructures have made significant progress in the fields of nano radio and television integration, superstructured materials and biosensors, but the performance and response mechanism of current metal nanostructures still need to be further studied and understood. Therefore, this study explored the hybrid mechanism of SPP of metal nanostructures and the factors affecting absorption characteristics. By combining a gold nanoparticle array with a Fabry Perot cavity, when the refractive index of the surrounding dielectric environment changed from 1.30 to 1.38 at intervals of 0.02, two reflection valleys shifted significantly towards the red, and the sensitivities of reflection valleys 2 and 3 were 300 nm/Refractive Index Unit (RIU) and 600 nm/RIU, respectively. The result indicated that the sensor exhibited high sensitivity in different refractive index environments. The study also designed a multiple partition multiplexing structure to verify the sensing performance of plasmon nanostructures in different refractive index environments. The research findings indicated that adjusting the width of the second dielectric layer influenced the absorption of specific modes, resulting in fluctuations in absorption intensity between 92% and 100%. The study revealed that the hybrid mechanism of SPPs in metal nanostructures, coupled with a Fabry-Perot cavity and gold nanoparticle array, exhibited high sensitivity to refractive index changes, offering potential for the development of highly responsive sensors in diverse environments.

Keywords: metal nanostructures; surface plasmon polariton; absorption properties; sensing properties; hybridization effects.

***Corresponding author:** Ruirui Zhang, School of Computer Science and Technology, Shandong University of Finance and Economics, Jinan 250014, Shandong, China. Email: zhangruirui0268@126.com.

Introduction

With the vigorous development of nanotechnology, plasmon hybridization on the surface of metal nanostructures and related absorption properties have become the focus of much attention in the disciplines of materials science and optics [1]. Although some important research results have been achieved, there are still a series of unresolved problems and unknown factors. First, the study of surface plasmon hybridization of metal nanostructures faces challenges between theory and experiment [2]. The establishment of theoretical models requires a more accurate description of the complex electromagnetic field distribution on the surface of nanostructures, while experimental methods require higher sensitivity and resolution

to capture small optical changes. This synergy between theory and experiment will provide in-depth understanding. Second, although the absorption properties of surface plasmons in metallic nanostructures have been studied to some extent, the absorption behavior under different materials, structures, and wavelength conditions is still unclear [3]. Therefore, in-depth study of the changes of absorption properties under different conditions is crucial for nanostructure design and performance optimization.

Surface Plasmon Polariton (SPP) hybridization of metal nanostructures can provide new design ideas and functional expansion for optical devices and nanophotonics. Khurana and Jaggi used transmission electron microscopy and scanning electron microscopy to characterize the morphology and size of nanostructures and measured the resonance wavelength and absorption properties of local surface plasmon resonance (LSPR) using UV visible spectroscopy [4]. To explore the property of dimers in metal nanostructures, Gerislioglu *et al*. conducted a study using Au dimers on Au substrates as an example [5]. By changing the dielectric environment of the dimer structure on the membrane, they observed a wide range of high-order mixed plasmon exciton families present in the visible spectrum. LSPR and Laser rangefinder (SLR) of dimer structure on a single film have highly sensitive response to refractive index. To overcome the limitations of surface coverage and particle aggregation on sensitivity and resolution of traditional LSPR fiber optic sensors, Lu *et al*. introduced a new self-assembly template technology [6]. Based on nano thickness block copolymers, a 33 nm single layer of gold nanoparticles was formed through a poly (styrene-b-4-vinylpyridine) layer, which had high uniformity and density and could be used for LSPR sensing. Dong and Bandaru investigated the interaction of specific surface plasmon modes by numerically simulating the behavior of surface plasmon modes [7]. In the metal dielectric metal arrangement, there were interactions between specific surface plasmon modes. Gupta and Banaszak had explored the interaction of specific surface plasmon modes in metal dielectric metal structures, studying their absorption spectra by studying geometric changes in nanostructures [8]. The absorption property of metal nanostructures offers a basis and support for the development of efficient energy conversion, precision medicine, and photonics applications. Wei *et al*. chose 2-anthraceneformic acid as the enantiomer of the head to head dimer, designed and prepared metal nanostructures, and manipulated molecular chirality by controlling their chirality [9]. The prochirality molecule 2-anthracoic acid was adsorbed on the metal nanohelix, and its enantiomeric preference was observed in photoinduced cyclodimerization. Wu *et al*. altered the properties of the dimer structure on the membrane by regulating its dielectric environment [10]. Characterization and analysis of LSPR and SLR of dimers were conducted by using spectroscopic techniques. Research has found that Au dimers on Au substrates had bright 'bonded' dimer plasmons and lower energy magnetic charge transfer plasmons. Sohal *et al*. studied the role and application of MnO_2 nanostructures in biosensors [11]. MnO_2 nanostructures were prepared using inexpensive, flexible, portable, and non-toxic electrode surfaces. Different forms of MnO_2 nanostructures were prepared and applied to electrochemical sensors. To solve the problem of how to improve optoelectronic devices and optical communication systems, Chen *et al*. used magnetic dipole resonance in metamaterial to enhance the broadband near-infrared absorption of single-layer graphene [12]. Through numerical simulation, it analyzed the optical absorption properties of single-layer graphene in metamaterial structure and realized the control of absorption properties by electrically modulating. To achieve customized design features, Bhattacharjee and Bose focused on the application of core-shell nanostructures in microwave absorption materials [13]. By adjusting the structure of its core and shell, microwave absorption enhancement was achieved, and the optical absorption properties of the electric modulation and switching unit of

single-layer Graphene in the near-infrared region were displayed.

Many scholars have studied the properties of metal nanostructures. Although there are already many theoretical models and computational methods used to describe and predict the optical properties of metal nanostructures, further improvement in their accuracy and reliability is still needed. Therefore, this study combined advanced theoretical models and experimental techniques and focused on the SPP and absorption of metal nanoparticles to deeply explore the hybridization mechanism of surface plasmons in metal nanostructures and the absorption properties related to them. By integrating theoretical models and advanced experimental techniques, this study aimed to reveal the microscopic distribution of electromagnetic fields on the surface of nanostructures and systematically study the effects of different parameters on plasmons to improve the resonance energy, absorption effect, and related properties. It was expected that the results of this study would help solving the current problems between theory and experiment and providing in-depth theoretical support and experimental guidance in the fields of nanophotonics, nano-optoelectronics, and sensor technology.

Materials and Methods

Preparation of SPPs materials based on prism coupling technology

The SPP is a phenomenon of electromagnetic wave coupling with free electronic oscillation on the metal interface. The electrons are excited to form SPP, which enhances the energy of the electromagnetic field at a specific frequency [14]. This resonance phenomenon can occur in different wavelengths such as visible and infrared light and is highly dependent on factors such as the shape, size, material, and refractive index of metal nanostructures, as well as the surrounding environment. The preparation of SPPs using prism coupling technology included multiple key steps. First, a suitable substrate was selected before a thin layer of highly conductive metal film, usually gold or silver, was precisely deposited on its surface. The characteristics of this metal film would directly affect the excitation effect of subsequent SPPs. Metal nanostructures were one of the key platforms to achieve perfect absorption, and the precise design and control of their properties were the key to experimental success. By using Fabry-Perot (FP) cavity resonance or localized surface plasmon resonance, efficient absorption of light of specific wavelengths or frequencies could be achieved. The core of this method was to match the photon frequency and the vibration frequency of metal nanoparticles or metal conduction electrons to achieve local field enhancement and reflection attenuation, which was expected to play an important role in fields such as solar energy collection. The study also designed a plasmonic biosensor structure, which was placed on a silica dielectric layer and contained an array of gold nanoparticles. These particles were arranged in the center of the FP cavity. The gold nanoparticle array exhibited periodic distribution in the x- and y-axis directions, and the specific periods were Px and Py, respectively. By incident light hitting the plasmonic nanostructure at a normal incident angle, its electric field direction was distributed along the long axis of the elliptical nanoparticle. The design of this structure could not only adjust the wavelength and absorption intensity of plasmon resonance, but also was expected to achieve specific detection and identification of biomolecules. The various parameters obtained from SPPs after preparation were listed in Table 1. By adding an opaque gold film with a thickness of 400 nm on the substrate, the transmission of light could be effectively eliminated, making the transmittance almost zero. Therefore, the absorptivity A could be expressed as A=1-R, where R was the reflectivity. The Metal-Dielectric-Metal (MDM) structure exhibited three absorption peaks at wavelengths of 661, 864, and 1,198 nm with absorption rates exceeding 99.9%, which made the MDM structure ideal as a perfect absorber for tri-band

Table 1. Simulation experiment parameter setting.

Serial number	High	Value	Width	Value
1	h_1	150	w_{x1}	426
2	h_2	100	w_{x2}	100
3	h_3	400	w_{x3}	600

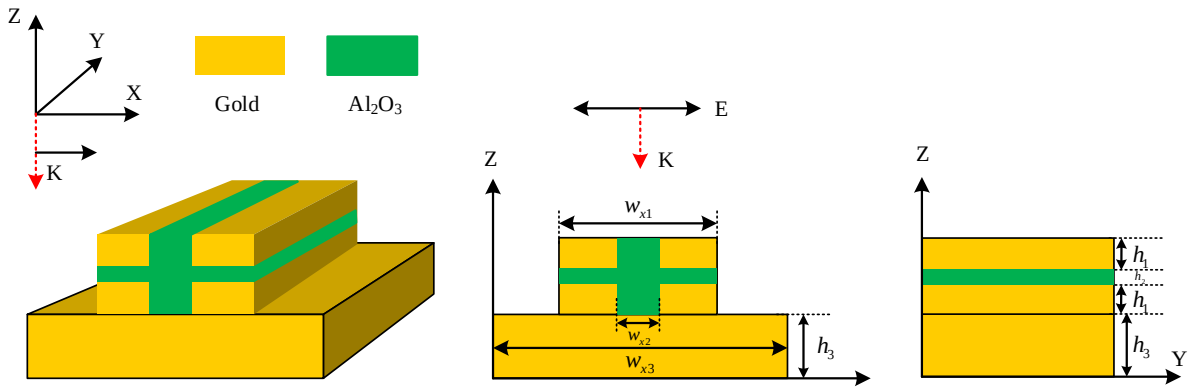

Figure 1. MDM structure.

plasmons. By combining the FP cavity resonance and the plasmon resonance effect in MDM nanostructures, perfect absorption could be achieved to effectively dissipate the incident energy by exciting magnetic and electrical resonances. To further improve the absorption efficiency and spectral control performance, the study proposed an MDM structure, which was composed of a gold grating, an Al_2O_3 grating composite layer, and a gold substrate, which achieved perfect absorption in three bands from visible light to near-infrared. Simulation studies using the finite difference time domain method showed that the realization of this structure mainly relied on the complex interactions between gap plasmon resonance, FP cavity resonance, LSPR, and SPPs. The designed MDM structure was shown in Figure 1, where the gold grating layer and Al_2O_3 grating layer played a key role. The gold grating layer was divided into horizontal and vertical Al_2O_3 grating layers. Figure 1 also showed a two-dimensional plane view of the XZ and YZ planes of the system. Among them, h_1, h_2, h_3 were gold and Al_2O_3 grating layer's thickness, and gold substrate, respectively. w_{x1} and w_{x2} were the width of the horizontal and vertical Al_2O_3 grating layers, while w_{x3} was the period per unit cell. A polarized plane wave propagating in the negative direction was used as the excitation source. The boundary conditions were applied to the periodic absorption layer in the x and y directions. The wavelength of the incident plane wave ranged from 0.6 to 1.4 pum. The study used a grid size of 8 nm × 8 nm × 8 nm, set the refractive index of Al_2O_3 to 1.76 and the surrounding medium to air. When comparing the effect of FP cavities on reflection spectra, experiments used gold nanoparticle arrays placed directly on a silicon dioxide substrate without FP cavities. The transmission spectrum normally was represented by the red solid line when light was incident. The blue dashed line represented the reflection spectrum of the FP cavity without gold nanoparticles.

Regulatory factors and mechanisms affecting the surface absorption properties of metal nanoparticles

The excitation of localized surface plasmons (LSPs) can generate strong electric field enhancement effects on the surface of nanoparticles, significantly improving the

efficiency of many nonlinear optical processes. For smaller sized nanoparticles $a = \lambda$, when placed in a uniform electrostatic field $E = E_0 r\cos\theta$, the internal electric field of the nanoparticles is E_{in} and the external electric field is E_{out}, while φ_{in} and φ_{out} represent the potential of the internal and external fields, respectively. The relationship between them can be represented by Equation (1).

$$\begin{cases} E_{in} = -\nabla\varphi_{in}, E_{out} = -\nabla\varphi_{out} \\ \nabla^2\varphi_{in} = 0(r < a), \nabla^2\varphi_{out} = 0(r < a) \end{cases} \quad (1)$$

When two different media meet, the potential value at their interface must be equal as shown in Equation (2).

$$\varphi_{in} = \varphi_{out}, \varepsilon\frac{\partial\varphi_{in}}{\partial r} = \varepsilon_m\frac{\partial\varphi_{out}}{\partial r}(r = a) \quad (2)$$

where ε was the dielectric constant of the particle. ε_m was the dielectric constant of the surrounding medium environment. In the model, the potential inside the metal ball was as follows.

$$\varphi_{in} = \frac{-3\varepsilon_m}{\varepsilon + 2\varepsilon_m} E_0 r\cos\theta \quad (3)$$

where E_0 was the incident electric field. ε was the dielectric constant of metal particles. ε_m was the dielectric constant of the surrounding environment. E_{in} was the electric field inside the particles. $\varphi_{in}(r,\theta)$ referred to the potential, where r was the position vector. The electric potential outside the metal ball was as:

$$\varphi_{out} = -E_0 r\cos\theta + a^3 E_0\frac{\varepsilon - \varepsilon_0}{\varepsilon + 2\varepsilon_m}\frac{\cos\theta}{r^2} \quad (4)$$

where φ_{out} was the potential energy of the incident electric field in Equation (3). After adding the total potential energy of the dipole in Equation (4), the dipole potential energy could be obtained as:

$$\varphi = \frac{p\cos\theta}{4\pi\varepsilon_m r^2} \quad (5)$$

Meanwhile, the dipole moment was shown in Equation (6).

$$p = 4\pi\varepsilon_m r a^3\frac{\varepsilon - \varepsilon_m}{\varepsilon + 2\varepsilon_m} E_0 \quad (6)$$

According to Equations (5) and (6), the polarizability of the dipole was obtained, which represented the degree of response of the material to an external electric field as shown in Equation (7).

$$\alpha = 4\pi a^3\frac{\varepsilon - \varepsilon_m}{\varepsilon + 2\varepsilon_m} \quad (7)$$

When the polarization reached the minimum value $|\varepsilon + 2\varepsilon_m|$, the system could achieve resonance enhancement effect, and the conditions for resonance enhancement were as:

$$\mathrm{Re}[\varepsilon(w)] = -2\varepsilon_m \quad (8)$$

Equation (8) was the dipole SPP resonance mode of metal nanoparticles. When the metal ball was placed in air, the resonance frequency $W_{LSP} = W_p/\sqrt{3}$ satisfied the Frohlich criterion. When in different dielectric environments, the resonance wavelength of LSPs would undergo a red shift phenomenon with changes in the dielectric constant ε_m. The relative displacement of LSPs wavelength and the change in refractive index were then shown in Equation (9).

$$\Delta\lambda = m\Delta n[1 - \exp(-2d/l_d)] \quad (9)$$

where *m* was the volume refractive index of the nanoparticles. Δn was the refractive index change of the surrounding adsorption medium.

d was the thickness of the effective adsorption layer. l_d was the attenuation length of the electromagnetic field. For both air and substrate media environments, there were usually two Rayleigh cutoff wavelengths, λ_p, corresponding to the disappearance distribution of air diffraction waves and the disappearance distribution of substrate diffraction waves, respectively [15]. For a square lattice whose lattice constant was a, when the incident plane passed through the base vector of the lattice, the expression of λ_r was shown in Equation (10).

$$\begin{cases} \lambda_{R\_m}^{sub} = \dfrac{a}{m}\left[n_s \pm \sin\theta\right] \\ \lambda_{R\_m}^{air} = \dfrac{a}{m}\left[1 \pm \sin\theta\right] \end{cases} \tag{10}$$

The Rayleigh cutoff wavelength in Equation (10) depends on the incident angle θ, integer m, and the refractive index n_s of the substrate. Therefore, when the Rayleigh cutoff wavelength λ_R approached the resonance wavelength of LSPs, LSPs and diffraction waves would form hybrid modes [16]. The condition for resonance to occur was $\varepsilon + 2\varepsilon_m \to 0$, which means that when the dielectric constant ε_m of the surrounding medium changed, the dielectric constant ε of resonance would also change accordingly [17]. According to the Drude model, assuming a damping constant of γ, the expression for resonance frequency could be derived as:

$$\omega_{LSPR} = \omega_p / \sqrt{2n_m^2 + 1} \tag{11}$$

According to the above relationship, the correlation between the formant position and the dielectric constant of the surrounding environment was shown in Equation (12).

$$\lambda_{LSPR} = \lambda_p / \sqrt{2n_m^2 + 1} \tag{12}$$

where n_m was the refractive index of the medium. $\lambda_{\max}$ and λ_p were the wavelength of the formant position and the plasmon frequency, respectively [18]. According to Mie's theory, the longitudinal plasmon formant of metal nanoparticles was shown in Equation (13).

$$\lambda_{LSPR} = \lambda_p / \sqrt{n_\infty + (1/\ p - 1)n_m} \tag{13}$$

where n_∞ was the dielectric constant of the metal and p was the depolarization factor. Relative sensitivity was defined as:

$$S_r = \frac{1}{\omega} \cdot \frac{\Delta\omega}{\Delta n} \times 100\% \tag{14}$$

where $\Delta\omega$ was the resonance frequency of metal nanoparticles in the air environment. The relative sensitivity of LSPR metal nanoparticles was shown in Equation (15).

$$FOM = \frac{1}{fwhm} \cdot \frac{\Delta\omega}{\Delta n} \tag{15}$$

where $fwhm$ was for the half width of the formant, in electronvolt (eV). SPPs also have characteristics against magnetic fields, and the magnetic resonance frequency can be increased by continuously reducing the size of the ring structure of SPPs. The development trend of plasmonic nanostructures was observed in the study, gradually extending from the initial microwave band to the terahertz and mid-infrared bands, and finally to the near-infrared region [19]. To verify this trend, experiments were conducted where the gold nanoparticle array was placed directly on a silicon dioxide substrate without an FP cavity and light was vertically incident. By showing the transmission spectrum of a gold nanoparticle array placed directly on the substrate and simultaneously comparing the reflection spectrum of the FP cavity without gold nanoparticles, the optical properties of plasmonic nanostructures in different wavelength bands could be derived.

Results and discussion

The SPP hybridization in metal nanostructures is a research hotspot, which involves the key issues of optical response and regulation. The interaction and coupling of SPP can be realized by introducing different materials or adjusting structural parameters on the surface of metal nanostructures to achieve accurate control of light absorption, scattering, and transmission [20]. This regulation technology has potential applications in optical devices, sensors, optical communication, and other fields, and provides a new idea for realizing efficient energy conversion and functional design of photonics devices.

SPP hybridization effect of metal nanostructures

Based on the structure proposed in the study, numerical calculation analysis was performed. The reflection spectrum of the FP cavity without gold nanoparticle array at normal incidence showed that a sharp reflection valley appeared at 714 nm, which was caused by the excitation of the first-order cavity mode (Figure 2). The electric field was greatly enhanced and was mainly localized in the central region of the optical cavity, which was also the factors for placing the gold nanoparticle array at the center of the FP microcavity. Only this configuration could make the cavity mode excitation in the FP cavity to produce an obvious strengthening of the electric field around the gold nanoparticles, thereby greatly promoting the LSPR excitation of the gold nanoparticles.

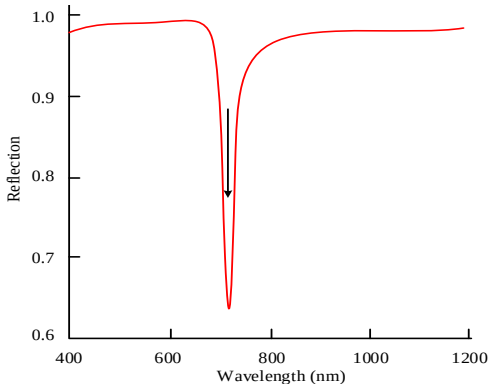

Figure 2. Reflectance spectrum of the FP cavity without the gold nanoparticle array at normal incidence.

There was a broadband transmission valley at the 684 nm position (transmission valley 1), which originated from the LSPR excitation of a single gold nanoparticle, and its bandwidth was significantly wider than the reflection spectrum of the FP cavity (Figure 3a). However, when the gold nanoparticle array was placed in the FP cavity, the plasmon resonance mode split into two ultra-narrow bandwidth hybrid plasmon modes (reflection valley 2 and reflection valley 3) (Figure 3b). The results suggested that there was a strong interaction between the cavity membrane of the FP cavity and the LSPR of the metal nanostructure, which resulted in the splitting and narrowing of the resonance peak, allowing the sensor to have a highly selective spectral response within a specific wavelength range. According to the structure designed in the study, the two hybridization modes had very narrow bandwidths. The widths of reflection valleys 2 and 3 were only 10.1 nm and 21.2 nm respectively, which were much smaller than typical LSPR.

To investigate the sensing properties of the designed plasmon nanostructures in different refractive index environments in detail, the refractive index of the surrounding dielectric environment was changed from 1.30 to 1.38 at intervals of 0.02. Two reflection valleys shifted significantly towards the red as the refractive index increased (Figure 4a). The relationship between the positions of reflection valleys 2 and 3 and the refractive index was shown in Figure 4b. By performing linear fitting, the sensitivities of reflection valleys 2 and 3 could be obtained with valley offsets of 300 nm/RIU and 600 nm/RIU, respectively. These results indicated that the sensitivity of metal nanostructures coupled with optical cavities was very high.

Verification of key factors and mechanisms for the absorption properties of metal nanostructures

Based on the proposed MDM structure, where R and T represented reflectance and transmittance, respectively, the absorption spectrum of this absorber was shown in Figure 5.

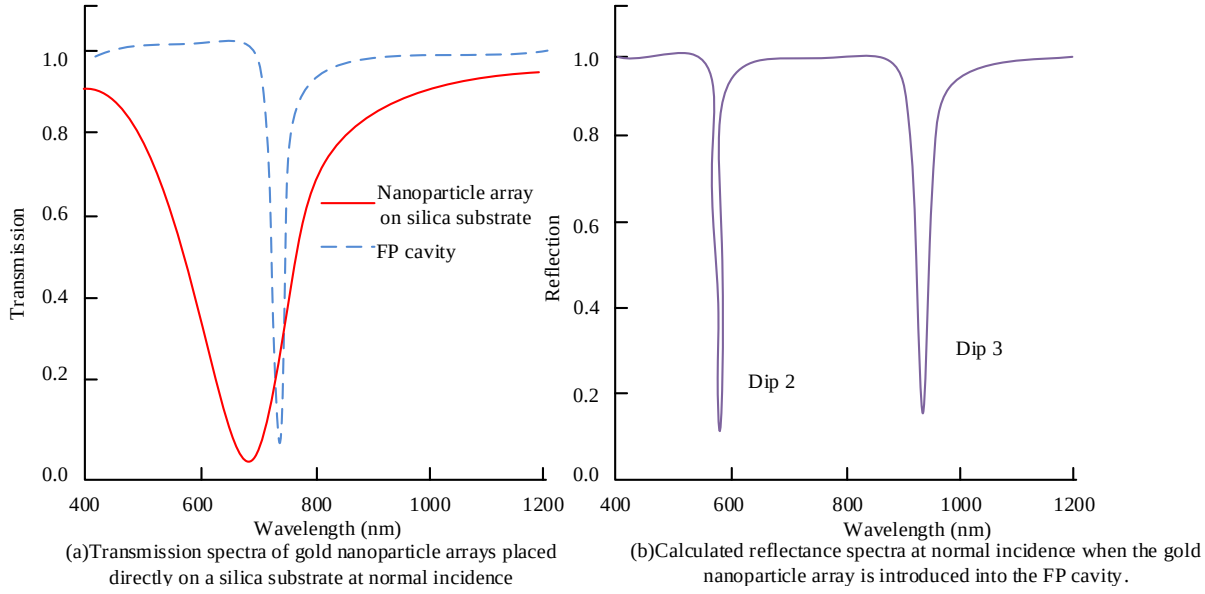

(a)Transmission spectra of gold nanoparticle arrays placed directly on a silica substrate at normal incidence

(b)Calculated reflectance spectra at normal incidence when the gold nanoparticle array is introduced into the FP cavity.

Figure 3. The transmission spectrum and the corresponding reflection spectrum.

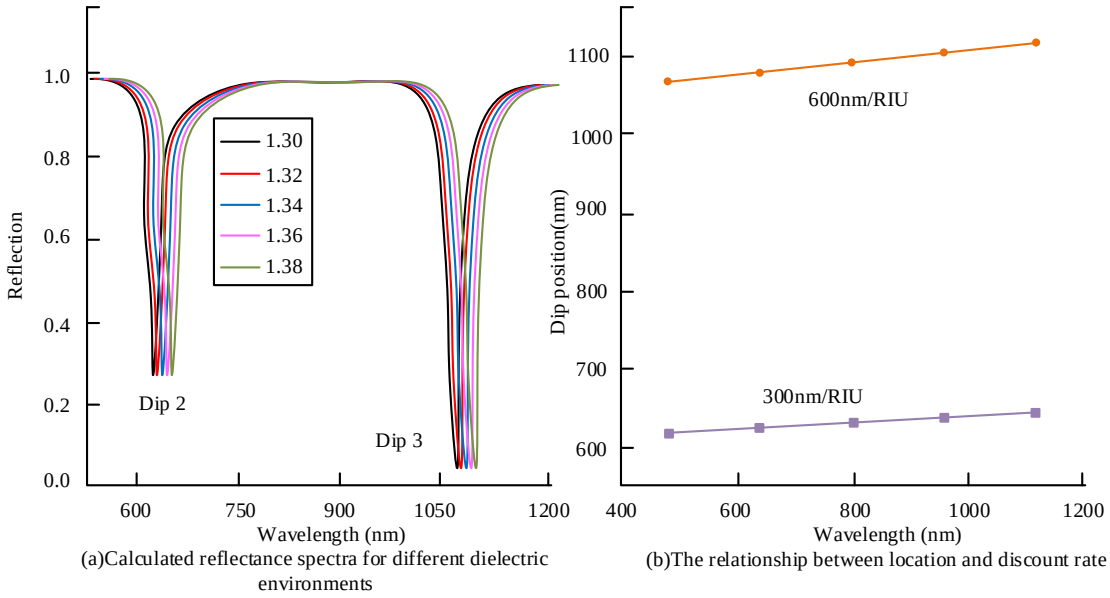

(a)Calculated reflectance spectra for different dielectric environments

(b)The relationship between location and discount rate

Figure 4. Sensing properties of plasmonic metal nanostructures.

The electric field distribution played a dominant role in analyzing the incident light's absorption. By studying the unit structure of MDM structure, the distribution of electric and magnetic fields at a wavelength of 661 nm was illustrated, where the gap PR between Al_2O_3 grating layers led to electric field density. At the wavelength of 864 nm, due to the excitation and coupling of the local SPP, the electromagnetic field was mainly confined to the gold grating slit and the corner of the metal strip of the adjacent unit.

By changing the thickness h_1 of the metal grating layer, the range was from 130 to 170 nm with intervals of 10 nm. The results denoted that the absorption peaks corresponding to modes 1, 2,

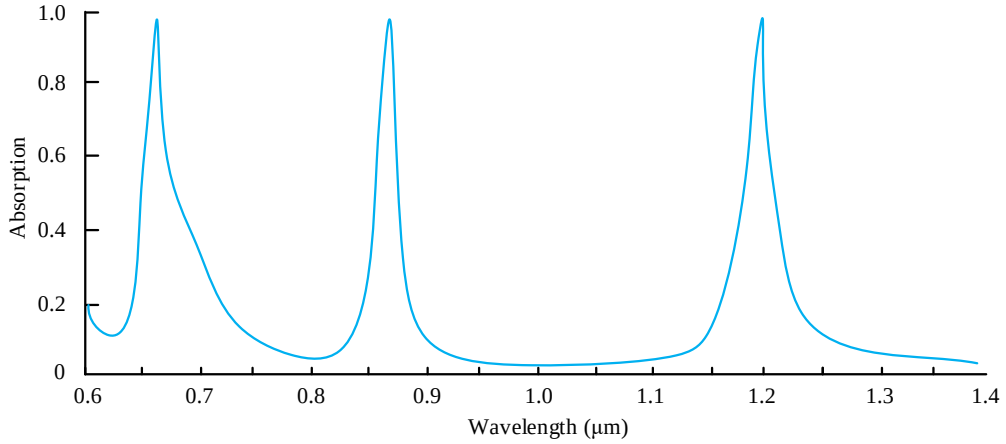

Figure 5. Absorption spectra of MDM structures based on parameters.

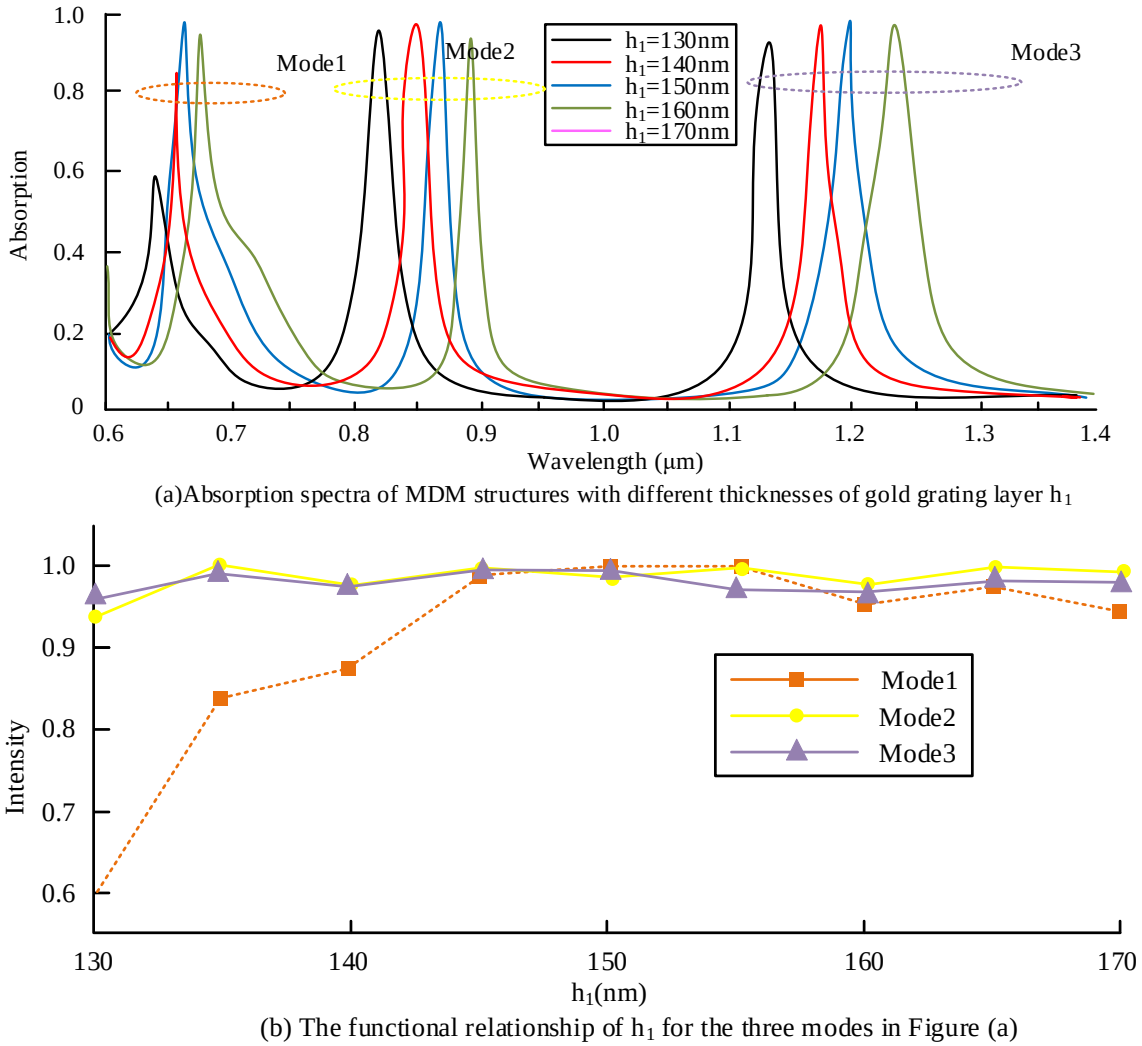

Figure 6. The absorption spectrum of the MDM structure with different thicknesses of the gold grating layer h1 and its corresponding h_1 function relationship.

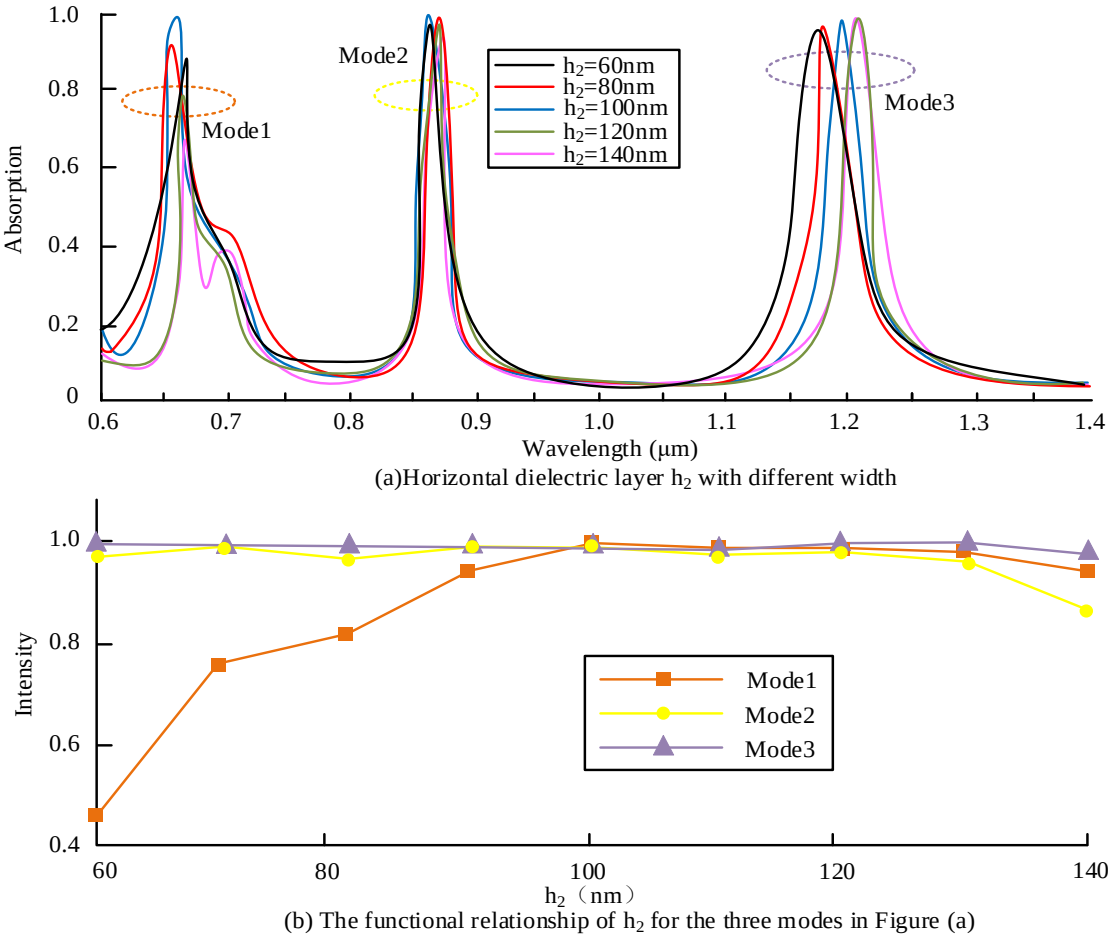

Figure 7. The absorption spectrum of the MDM structure with different thicknesses of the gold grating layer h_2 and its corresponding h_1 function relationship.

and 3 shifted red with the increase of h_1, and the absorption rates of each mode showed different responses to the changes in h_1 (Figure 6). As h_1 increased from 130 to 170 nm, the absorption of mode 1 first increased to 100% and then decreased to 95%, which indicated that the thickness h_1 of the metal grating layer had a significant impact on the absorption performance of the structure.

The change trend of the absorption spectrum with the change of h_2 and the relationship between the corresponding resonance absorption peak of each mode and h_2 were shown in Figure 7. According to the simulation results, as the thickness of the horizontal dielectric layer h_2 raised, the interaction between the metal and the dielectric grating layers increased, thereby improving the overall absorption capacity of the MDM structure (Figure 7a). For mode 1, the absorption rate of h_2 increased rapidly from 46% to 100% and then decreased from 100% to 94% when the h_2 increased from 60 to 140 nm (Figure 7b). However, modes 2 and 3's absorption rates were almost always near 100%, independent of the increase in h_2.

The absorption spectrum evolution of MDM structure at different vertical dielectric layer widths w_{x1} was displayed in Figure 8. The irregular fluctuations of the resonance wavelength of each mode as a function of w_{x1} was shown in Figure 8a, while the functional

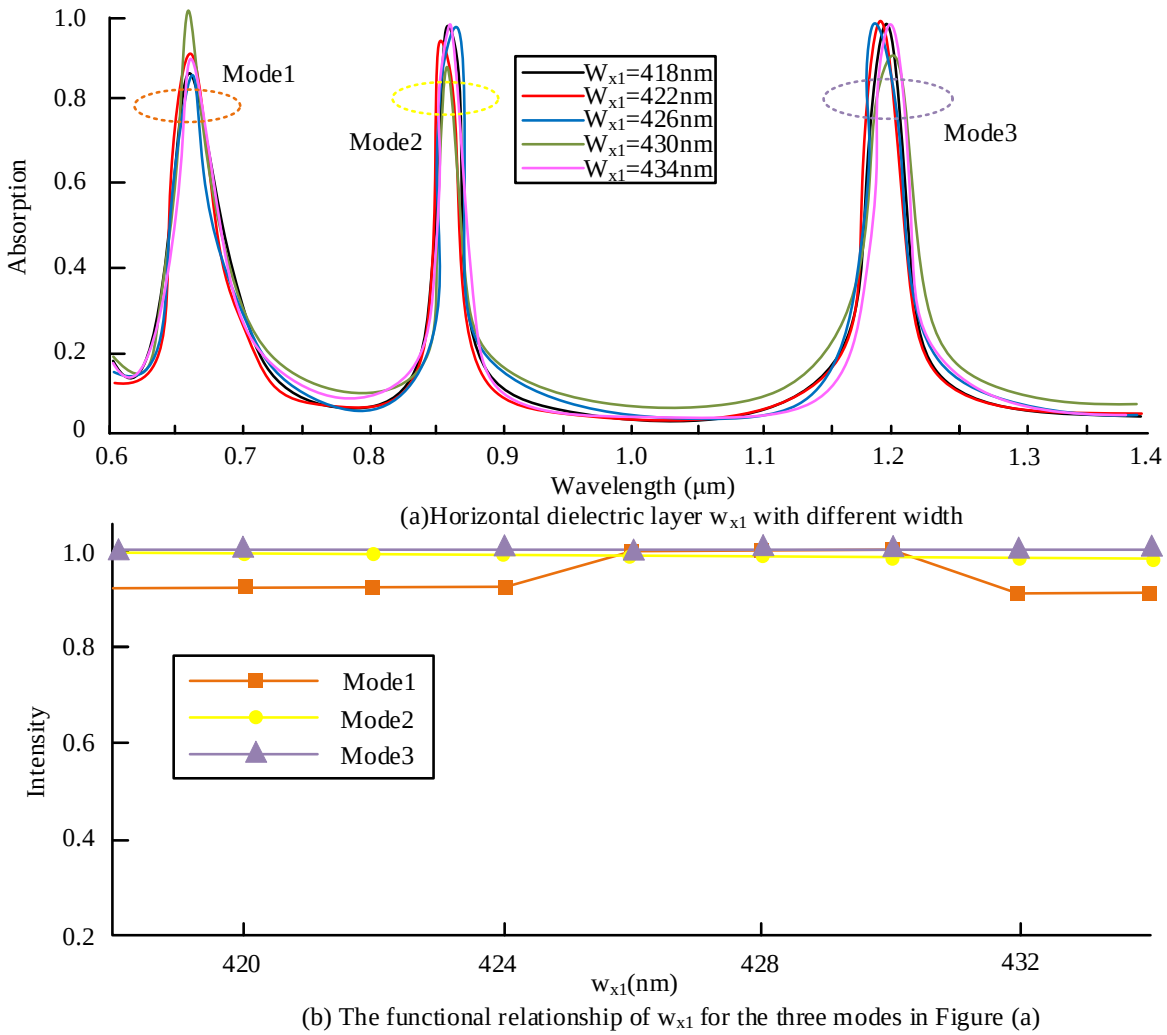

Figure 8. Vertical dielectric layer wx1 and its corresponding w_{x1} function relationship.

relationship between the peak absorption intensity and the vertical dielectric layer width w_{x1} was shown in Figure 8b. The peak absorption intensity of Modes 1, 2, and 3 could all reach over 80%, which indicated that the MDM structure had high stability and tolerance for changes in the vertical dielectric layer width w_{x1}.

The MDM structure was very sensitive to changes in the vertical dielectric layer width w_{x2}, resulting in significant fluctuations in the absorption spectrum (Figure 9). When the vertical dielectric layer width w_{x2} reached 100 nm, the absorption intensity of all three modes reached 100%, which indicated that, under a specific vertical dielectric layer thickness, the MDM structure could achieve efficient light absorption, and fine-tuning the vertical dielectric layer width w_{x2} could effectively adjust and optimize the absorption performance of the MDM structure.

The effect of grating period w_{x3} on the absorption spectrum of MDM structure was shown in Figure 10a. As the grating period w_{x3} increased from 500 to 700 nm, the resonance wavelengths of modes 1 and 3 underwent a redshift phenomenon, while that of Mode 2 remained almost unchanged. This phenomenon indicated that the grating period w_{x3} had a significant impact on the resonance properties of different modes. Further, the

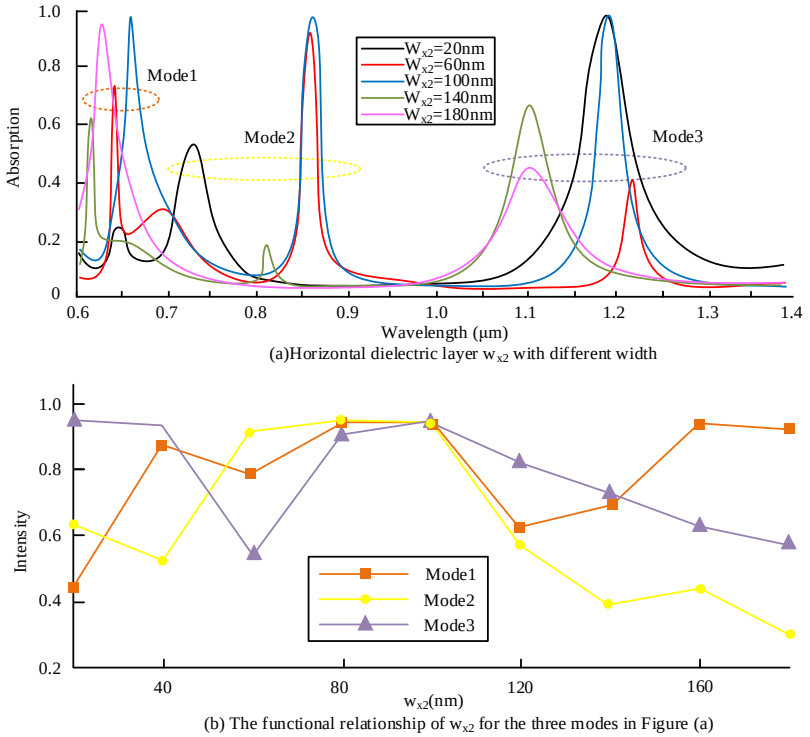

Figure 9. The vertical dielectric layer w_{x2} and its corresponding w_{x2} function relationship.

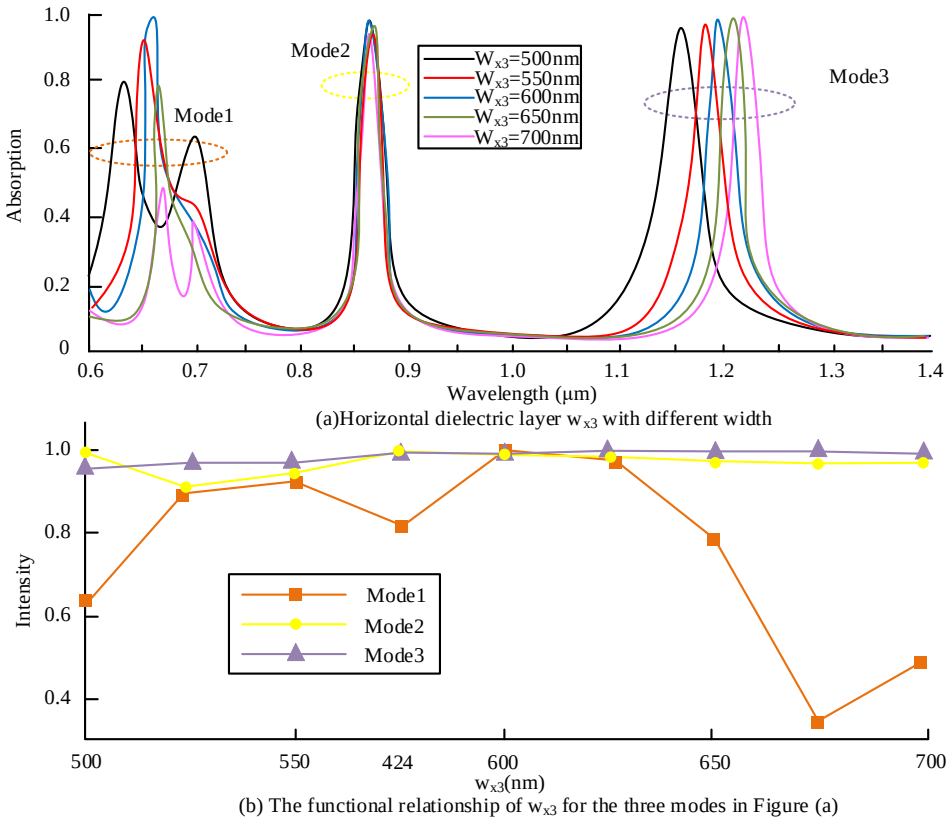

Figure 10. The vertical dielectric layer w_{x3} and its corresponding w_{x3} function relationship.

absorption intensities of modes 1, 2, and 3 were all affected by the grating period w_{x3}, especially, when the grating period w_{x3} was 500 nm, 550 nm, and 700 nm, the absorption peak of mode 1 split into two peaks (Figure 10b).

Conclusion

SPPs are electromagnetic waves excited at the interface between metal and dielectric materials. Its existence leads to local electromagnetic field enhancement and energy concentration. This study proposed to combine metal nanostructures with other materials to form composite structures to control their plasmonic properties. The plasmon hybridized metal nanostructures could be obtained through spectroscopic techniques, electrical testing, and microstructure characterization, which could also be carried out through numerical simulation and theoretical analysis. Under different refractive index environments, the reflection valleys on the surface of metal nanostructures showed obvious red shifts. Specifically, the sensitivities of reflection valleys 2 and 3 reached 300 nm/RIU and 600 nm/RIU, respectively. The change in the width of the vertical dielectric layer (w_{x2}) affected the absorption intensity of each mode, and when (w_{x2}) was 100 nm, the absorption intensity of Mode 1, 2, and 3 reached the maximum. In addition, the change of the grating period (w_{x3}) caused the resonant wavelength of Modes 1 and 3 to red shift, indicating that the absorption intensity was jointly affected by (w_{x2}) and (w_{x3}). Further research also needs to explore and optimize more experiments to achieve more precise control.

References

1. Dai Y, Ghosh A, Yang S, Zhou Z, Huang C, Petek H. 2022. Poincaré engineering of surface plasmon polaritons. Nat Rev Phys. 4(9):562-564.
2. Guo YJ, Xu KD, Deng X, Cheng X, Chen Q. 2020. Millimeter-wave on-chip bandpass filter based on spoof surface plasmon polaritons. IEEE Electr Device L. 41(8):1165-1168.
3. Bandewad G, Datta KP, Gawali BW, Pawar SN. 2023. Review on discrimination of hazardous gases by smart sensing technology. Artif Intell Appl. 1(2):86-97.
4. Khurana K, Jaggi N. 2021. Localized surface plasmonic properties of Au and Ag nanoparticles for sensors: A review. Plasmonics. 16(4):981-999.
5. Gerislioglu B, Dong L, Ahmadivand A, Hu H, Nordlander P, Halas N. 2020. Monolithic metal dimer-on-film structure: New plasmonic properties introduced by the underlying metal. Nano Lett. 20(3):2087-2093.
6. Lu M, Peng W, Lin M, Wang F, Zhang Y. 2021. Gold nanoparticle-enhanced detection of DNA hybridization by a block copolymer-templating fiber-optic localized surface plasmon resonance biosensor. Nanomaterials. 11(3):616-625.
7. Dong Y, Bandaru PR. 2020. Interaction and hybridization of orthogonal Fabry-Pérot like surface plasmon modes in metal-dielectric grating structures. Opt Express. 28(3):3541-3551.
8. Gupta S, Banaszak A. 2021. Detection of DNA bases and environmentally relevant biomolecules and monitoring ssDNA hybridization by noble metal nanoparticles decorated graphene nanosheets as ultrasensitive G-SERS platforms. J Raman Spectrosc. 52(5):930-948.
9. Wei X, Liu J, Xia GJ, Deng J, Peng S, Jason J, *et al*. 2020. Enantioselective photoinduced cyclodimerization of a prochiral anthracene derivative adsorbed on helical metal nanostructures. Nat Chem. 12(6):551-559.
10. Wu N, Du W, Hu Q, Jiang S. 2020. Recent development in fabrication of Co nanostructures and their carbon nanocomposites for electromagnetic wave absorption. Eng Sci. 13(19):11-23.
11. Sohal N, Maity B, Shetti NP, Basu S. 2021. Biosensors based on MnO2 nanostructures: A review. ACS Appl Nano Mater. 4(3):2285-2302.
12. Chen J, Chen S, Gu P, Yan Z, Tang C, Xu Z, *et al*. 2020. Electrically modulating and switching infrared absorption of monolayer graphene in metamaterials. Carbon. 162(2):187-194.
13. Bhattacharjee Y, Bose S. 2021. Core–shell nanomaterials for microwave absorption and electromagnetic interference shielding: A review. ACS Appl Nano Mater. 4(2):949-972.
14. Monticone F. 2021. A truly one-way lane for surface plasmon polaritons. Nat Photonics. 14(8):461-465.
15. Serafinelli C, Fantoni A, Alegria ECBA, Vieira M. 2022. Plasmonic metal nanoparticles hybridized with 2D nanomaterials for SERS detection: A review. Biosensors. 12(4):225-248.
16. Guan J, Park JE, Deng S, Tan M, Hu J, Odom T. 2022. Light–matter interactions in hybrid material metasurfaces. Chem Rev. 122(19):15177-15203.
17. Wang K, Zhou H, Luan X, Hu S, Zhou X, He S, *et al*. 2021. $NaTaO_3$ microwave dielectric ceramic a with high relative permittivity and as an excellent compensator for the temperature coefficient of resonant frequency. Ceram Int. 47(1):121-129.
18. Kang ESH, Chen S, Derek V, Hagglund C, Eric D, Jonsson P. 2021. Charge transport in phthalocyanine thin-film transistors coupled with Fabry–Perot cavities. J Mater Chem C. 9(7):2368-2374.

19. Geng X, Ding H, Wei K, Chen L. 2020. Suppression of multiple modal resonances of a cantilever beam by an impact damper. Appl Math Mech. 41(3):383-400.
20. Fregoni J, Haugland TS, Pipolo S, Giovannini T, Koch H, Corni S. 2021. Strong coupling between localized surface plasmons and molecules by coupled cluster theory. Nano Lett. 21(15):6664-6670.